INTERNATIONAL JOURNAL OF RENEWABLE ENERGY RESEARCH
A. EL-ABIDI *et al.* ,*Vol. 9, No. 2, June, 2019*

Assessment of Hourly Solar Direct Normal Irradiance using Eight Broadband Clear Sky Models: Study of Four Moroccan Arid Sites

Abderrahim El-Abidi*, **‡, Said Yadir*, **, Mohammadi Benhmida**, Hamza Bousseta*, Wail El Bazi***, Abdelilah Faké****, Kamal Baraka*****

*Laboratory of Materials, Processes, Environment, and Quality (LMPEQ), ENSA-SAFI, Cadi Ayyad University, Route Sidi Bouzid, BP 63, 46000, Safi, Morocco

**Laboratory of Electronics, Instrumentation and Energetic, Faculty of Sciences, Chouaïb Doukkali University, B.P 20, El Jadida, Morocco

*** LIPOZY, ENSA-Khouribga, Sultan Moulay Slimane University, BéniMellal, Morocco

*****Department of Physics, Faculty of Sciences, Chouaïb Doukkali University, B.P 20, El Jadida, Morocco

**** Mathematical Research and Information Processing Team, Sidi Bouzid, BP 63, 46000, Safi, Morocco

(a.elabidi@uca.ma, yadir1976@yahoo.fr, benhmida@gmail.com, hamza.bousseta@gmail.com, w.elbazi@usms.ma, baraka.kamal@yahoo.fr fak_abdelilah@yahoo.fr)

‡ Abderrahim El-Abidi; Said Yadir, Route Sidi Bouzid, BP 63, 46000, Safi,Morocco

Tel: +212 664088042, Fax: +212 24 66 80 12, a.elabidi@uca.ma

Received: 12.04.2019 Accepted: 27.05.2019

Abstract- This paper presents a statistical comparative study of eight important parametric broadband clear sky models, against Meteosat-derived data, to estimate solar hourly direct normal irradiance (DNI) for four Moroccan arid zone sites. To achieve this aim, four sites well spread across this climatic zone were selected, and four references days were chosen. The statistical parameters such as relative mean bias error (rMBE), the relative root mean square error (rRMSE), and the determination coefficient R^2 are calculated. According to these results, the Bird model produces acceptable estimates with 62.5% of good results of rMBE ranging between 0 and 6%; 25% of average results of rRMSE ranging between 11% and 14%, and 62.5% of good results of R^2 ranging between 0.90 and 0.96. The comparison of both means of DNI, calculated and measured for a given site and day of reference, using the paired t-test, states that for a level of significance of 1%, the Bird model and the REST2 model give in the quarter of the studied cases conforming means of hourly DNI. For a level of significance of 0.1%, the Bird model is more proficient and gives conforming means in almost half of the cases studied. Despite all these performances displayed by the Bird Model, it remains average and does not reach the required level in some sites at certain times. The elaboration of a new simpler DNI estimation model giving higher performances for this zone of high solar potential is of great interest.

Keywords: Clear sky model, direct normal irradiance (DNI), Moroccan arid zone, modeling, solar energy, statistical comparison.

1. Introduction

Morocco has a very great solar potential with incident solar energy averaging 4.7 to 5.7 kWh/m² per day [1]. Thus, it has established a solar program "Noor", estimated at 9 billion dollars, with the aim of producing 2,000 MW of solar power by 2020[2]. This program is characterized by the construction of thermodynamic concentrated solar power (CSP) and photovoltaic plants all located in the arid and desert zone of the country. Since the direct normal irradiance (DNI) is the component of global solar coming from the solid angle of the suns disk[3] and mainly focused by CSP [4], the modeling of this component of solar radiation in this zone characterized by an annual DNI potential higher than 2,000 kWh/m² [5] is of a great interest. Thus, the determination of the mathematical model describing the DNI by giving more accurate estimates will help in the planning of this solar power plants , their conception and optimal utilization [4]-[6].

Recently, many studies have been devoted to the validation of the Meteosat Second Generation MSG derived data. Marchand et al [7] validated the Copernicus Atmosphere Monitoring Service (CAMS-rad) version 3.2 databases by comparing them to coincident ground measurements made at five stations in Morocco. The five compared stations are all located in Moroccan arid or semi-arid zone. Given the scarcity of data concerning this zone, one can consider that the fewer uncertainties observed will not influence the comparative study of broadband models to estimate hourly DNI against data generated using CAMS-rad version 3.2. Table.1 regroup the selected sites for this study. All are well spread over the Moroccan arid zone. The Bird, Atwater & Ball, Paltridge &Platt, Linke-Kasten, Hoyt, Ineichen & Perez, Molineaux, and REST2 models are the Broadband parametric models selected to achieve this study. All are simpler parametric models and are the most recommended in literature to estimate DNI. Note that using theses models the estimation of the DNI is possible using only meteorological parameters as inputs [8]-.

The main objective of this work is to study and apply these broadband models to Morocco's arid climate zone. Four sites well distributed in this climatic zone of very high solar potential were selected and four reference days equitably distributed over time, which are the two solstices and the two equinoxes, were considered.

Table 1. Geographical coordinates of the four studied sites having arid zone[5].

	Latitude φ	Longitude	Altitude	Annual DNI
Ouarzazate	30.92°	-6.89°	1120	2,458
Errachidia	31.92°	-4.44°	1033	2,270
Guelmime	28.99°	-10.04°	313	2,098
Tendrara	33.05°	-2.00°	1443	2,246

2. Models, data used and Methods

2.1. Tested models

- *Bird model*

The direct normal irradiance I_{bn} in this model is given by[9]:

$$I_{bn} = 0.9662 \times I_{sc} \times \tau_R \times \tau_o \times \tau_u \times \tau_w \times \tau_A \quad (1)$$

In our calculations we used in Eq.1 factor 0.9751 instead of 0.9662 as adjusted by Bird. Iqbal et al used this modified formulation in his model of estimation of the global irradiance[10].

I_{sc} stands for extraterrestrial solar radiation in eq.1. It is estimated using the following equation:

$$I_{sc} = I_0\left[1 + 0.033 \times \cos\left(360\left(n_j - 2.7206\right)/365.25\right)\right] \quad (2)$$

I_0 denotes the solar constant, which is equal to 1,367 W/m², and n_j denotes the day number of the year, ranging from 1 on 1 January to 365 on December 31.

τ_R , is the transmittance functions for Rayleigh scattering and is given by [11]:

$$\tau_R = \exp\left\{-0.0903(M')^{0.84} \times \left[1 + M' - (M')^{1.01}\right]\right\} \quad (3)$$

Where:

M' is the pressure corrected air mass and expressed as follows:

$$M' = M \times e^{-0.0001148 \times z} \quad (4)$$

z is the altitude in (m) of the location studied, M is the air mass and is given by Kasten [12]-[13]:

$$M = \frac{1}{\sin(h) + 0.15 \times (3.885 + h)^{(-1.253)}} \quad (5)$$

Where h is the solar altitude in (rad).

τ_u is the absorption by the uniformly mixed gases (oxygen and carbon dioxide). It is expressed as follows [11]:

$$\tau_u = \exp\left(-0.0127 \times M'^{0.26}\right) \quad (6)$$

τ_o is the ozone absorption and given by [11]:

$$\tau_o = 1 - 0.1611 X_0 \times (1 + 139.48 X_0)^{-0.3035} - 0.002715 \times X_0\left(1 + 0.044 X_0 + 0.0003 X_0^{\,2}\right)^{-1} \quad (7)$$

Where, X_0 is the total amount of ozone in a slanted path (atm.cm)

$$X_0 = U_0 \times M \quad (8)$$

U_0 is the Amount of ozone in a vertical column from surface in $(matm - cm)$ for any location in the earth's northern hemisphere is given by[14]:

$$U_0 = 235 + \sin^2(1.28\varphi) \times \begin{bmatrix} 150 + \\ 40\sin\left(0.9865\left(n_j - 30\right)\right) \\ +20\sin\left(3L + I\right) \end{bmatrix} \quad (9)$$

Where, φ and L are the latitude and the longitude of the site in (rad), respectively. And $I = 0$ if the longitude of the location is "West", and $I = 20$ if it is "East".

τ_w is the water vapor absorption. It is given by [11]:

$$\tau_w = 1 - 2.4959 \times X_w\left[\left(1 + 79.03 \times X_w\right)^{0.6828} + 6.385 \times X_w\right]^{-1} \quad (10)$$

Where, X_W is the total of precipitable water in a slanted path (cm.H2O), it is expressed as:

$$X_W = w \times M \quad (11)$$

w in (cm) is the Amount of precipitable water in a vertical column from surface is given by[15]

$$w = \frac{49{,}953}{T} \times HR \times 10^{\left(17.443 - \frac{2{,}795}{T} - 3.868 \times Log(T)\right)} \quad (12)$$

T is the ambient temperature in (K). HR is the relative humidity.

τ_A is the aerosol extinction and given by [11]:

$$\tau_A = \exp\left[-K_A^{0.873} \times \left(1 + K_A - K_A^{0.7088}\right) \times M^{0.9108}\right] \quad (13)$$

Where,

$$K_A = 0.2758 \times K_{A,0.38} + 0.351 \times K_{A,0.5} \quad (14)$$

$K_{A,0.38}$ is the Aerosol optical depth from surface in a vertical path at $\lambda = 0.38\ \mu m$

$K_{A,0.5}$ is the Aerosol optical depth from surface in a vertical path at $\lambda = 0.5\ \mu m$

The two latest dimensionless coefficients are determined using the formula proposed by Angstrom[9]:

$$K_A(\lambda) = \beta \times \left[\lambda(\mu m)\right]^{-\alpha} \quad (15)$$

β is the Angström's turbidity coefficient and α is the wavelength exponent.

For $\lambda = 0.38\ \mu m$ we took $\alpha = 1.0274$

For $\lambda = 0.5\ \mu m$ we take $\alpha = 1.2060$

- *Atwater and Ball model*

The direct normal irradiance I_{bn} given by Atwater and Ball model is represented as [16]:

$$I_{bn} = I_{sc} \times (\tau_M - a_w) \times \tau_A \quad (16)$$

Where, τ_M is the transmittance for all molecular effects except water vapor absorption and given by:

$$\tau_M = 1.041 - 0.15\left[M \times \left(949.10^{-8} P + 0.051\right)\right]^{0.5} \quad (17)$$

P is the atmospheric pressure in (Pa), M is calculated using the expression given in the Eq.5.

The absorptivity by water vapor a_w is given as:

$$a_w = 0.077\left(w \times M\right)^{0.3} \quad (18)$$

We note that we used the expression of w already defined in the Eq.12 in the calculation of a_w. The transmittance τ_A after aerosol attenuation is given as:

$$\tau_A = \exp(-M' \times K_A) \quad (19)$$

K_A is defined by the Eq.14 previously given in the Bird model.

- *Paltridge & Platt model*

The direct normal irradiance I_{bn} of the Paltridge & Platt model is given by[17]:

$$I_{bn} = I_{sc} \times (\tau_0 \times \tau_R - a_w) \times \tau_A \quad (20)$$

Hay and Davies have used this expression in their global solar irradiance model[18]. A number of authors have contributed to the development of this model[10]. Paltridge and Platt recommended the formalism of the transmittance function of ozone absorption τ_o, and the absorptivity by water vapor τ_w, given by Lacis and Hansen in their model for the global irradiance. Therefore,

$$\tau_0 = 1 - \left[\frac{0.02118X_0}{1 + 0.042X_0 + 0.000323X_0^2} + \frac{1.082X_0}{\left(1 + 138.6X_0\right)^{0.805}} + \frac{0.0658X_0}{\left(1 + 103.6X_0\right)^3}\right] \quad (21)$$

$$a_w = 2.9X_w / \left(1 + 141.5X_w\right)^{0.635} + 5.925X_w \quad (22)$$

Where the expression of X_0 and X_w are given by the Eq.8 and Eq.11, respectively.

The attenuation due to Rayleigh scattering τ_R can be evaluated through the Eq.3 given by Bird. The transmission after the aerosol extinction τ_A can be evaluated for $\beta < 0.5$ through the Maächler equation[10]:

$$\tau_A = \left(0.12445\alpha - 0.0162\right) + \left(1.003 - 0.125\alpha\right) \times \exp\left[-\beta M'\left(1.089\alpha + 0.5123\right)\right] \quad (23)$$

The coefficient α was fixed at the value of 1.3 [10].

- *Linke - Kasten model*

This Model is very often called Kasten model. In fact, the expression of direct normal irradiance is given by Linke [19]-[20]:

$$I_{bn} = I_{sc} \times \exp\left(-\delta_R \times M' \times T_L\right) \quad (24)$$

The expression of δ_R used in this model is defined by [21] as follows:

$$\delta_R = \frac{1}{0.9 \times M' + 9.4} \tag{25}$$

Therefore, we preferred to name this model with the association of these two names.

- *Hoyt model*

From this model the direct normal irradiance is given by [22]:

$$I_{bn} = I_{sc} \times \left(1 - \sum_{i=1}^{5} a_i\right) \tau_R \tau_A \tag{26}$$

Where the parameters a_1, a_2, a_3, a_4, a_5 are the absorbance parameters defined by Hoyt as follows:

$$a_1 = 0.110 \times (0.75 U_w M + 6.31 \times 10^{-4})^{0.3} - 0.0121 \tag{27}$$

$$a_2 = 0.00235 \times (136 M' + 0.0129)^{0.26} - 7.5 \times 10^{-4} \tag{28}$$

$$a_3 = 0.045 \times (U_0 M + 8.34 \times 10^{-4})^{0.38} - 3.1 \times 10^{-3} \tag{29}$$

$$a_4 = 7.5 \times 10^{-3} \times (M')^{0.875} \tag{30}$$

$$a_5 = 0.05 \times T_A \tag{31}$$

The transmittance due to Rayleigh scattering τ_R is calculated here by the following equation instead of the tabulated form used by Hoyt[10]:

$$\tau_R = 0.6175975 + 0.375566 \exp(-0.2211875 M') \tag{32}$$

The transmittance of aerosol scattering is given by:

$$\tau_A = [g(\beta)]^{M'} \tag{33}$$

Where:

$$g(\beta) = -0.914000 + 1.909267 \exp(-0.667023 \times \beta) \quad with\ 0 < \beta < 0.5 \tag{34}$$

- *Ineichen and Perez model*

This model was developed by Inchein and Perez[19] in 2002 and is given by the expression:

$$I_{bn} = b \times I_{sc} \times \exp\left(-0.09 \times M' \times (T_L - 1)\right) \tag{35}$$

Where b is a multiplicative coefficient depending on the altitude of the location and is given by:

$$b = 0.664 + \left(0.163 \times \exp(z / 8{,}000)\right) \tag{36}$$

- *Molineaux model*

In This model the direct normal irradiance is given by Molineux et al [23] as follows:

$$I_{bn} = I_{sc} \times \exp\left(-\Delta_{cda} \times T_L \times M'\right) \tag{37}$$

Where Δ_{cda} is the integrated optical thickness of a clean and dry atmosphere, and is given by:

$$\Delta_{cda} = 0.124 - 0.0285 \times \log(M') \tag{38}$$

- *REST2 Model*

In this Model, the solar spectrum is subdivided into two bands. The first is of ultraviolet and visible and the second is of the infrared. The direct normal irradiance I_{bn} is the sum of two-band components: I_{bn1} and I_{bn2}. Each of these is calculated using the following expression [24]:

$$I_{bni} = I_{sci} \times \tau_{Ri} \times \tau_{ui} \times \tau_{Oi} \times \tau_{Ni} \times \tau_{Wi} \times \tau_{Ai} \tag{39}$$

Where τ_{Ri}, τ_{ui}, τ_{Oi}, τ_{Ni}, τ_{Wi}, and τ_{Ai} are the band transmittances for Rayleigh scattering, uniformly mixed gas absorption, ozone absorption, nitrogen dioxide absorption, water vapor absorption and aerosol extinction, respectively. The energies contained in bands Band 1 and Band 2 are respectively:

$$I_{sc_1} = 0.4604 \times I_{sc} \text{ and } I_{sc_2} = 0.5057 \times I_{sc} \tag{40}$$

The following equations give the formulation of different transmittances in the two bands[24]:

- ***In band 1:***

$$\tau_{R_1} = \frac{(1 + 1.8169 M' - 0.033454 M'^2)}{(1 + 2.063 M' + 0.31978 M'^2)} \tag{41}$$

$$\tau_{g_1} = \frac{(1 + 0.95885 M' + 0.012871 M'^2)}{(1 + 0.9632 M' + 0.015444 M'^2)} \tag{42}$$

$$\tau_{o_1} = (1 + f_1 m_o + f_2 m_o^2)/(1 + f_3 m_o) \tag{43}$$

$$\tau_{n_1} = Min[1, (1 + g_1 m_w + g_2 m_w^2)/(1 + g_3 m_w)] \tag{44}$$

$$\tau_{w_1} = (1 + h_1 m_w)/(1 + h_2 m_w) \tag{45}$$

$$\tau_{a_1} = \exp\left(-m_a \times \beta_1 \times \lambda_{e_1}^{\alpha_1}\right) \tag{46}$$

- ***In band 2 :***

$$\tau_{R_2} = \frac{(1 - 0.010394 M')}{(1 - 0.00011042 M'^2)} \tag{47}$$

$$\tau_{g_2} = \frac{(1 + 0.27284 M' - 0.00063699 M'^2)}{(1 + 0.30306 M')} \tag{48}$$

$$\tau_{o_2} = 1 \ ; \ \tau_{n_2} = 1 \tag{49}$$

$$\tau_{w_2} = \frac{(1 + c_1 m_w + c_2 m_w^2)}{(1 + c_3 m_w + c_4 m_w^2)} \tag{50}$$

$$\tau_{a_2} = \exp\left(-m_a \times \beta_2 \times \lambda_{e_2}^{\alpha_2}\right) \tag{51}$$

m_o, is the ozone optical mass, m_w is the water vapor optical mass , and m_a is the aerosol optical mass are given by[25]:

$$m_o = 13.5 / \sqrt{181.25 \times \sin^2(h) + 1} \tag{52}$$

$$m_w = \left[\sin(h) + 0.0548(h + 2.65)^{-1.452}\right]^{-1} \tag{53}$$

$$m_o \simeq m_w \tag{54}$$

f_1, f_2, and f_3 are parameters depending on U_0 the Ozone column amount[24]. g_1, g_2, and g_3 are parameters depending on the U_n [24], the total column amount of NO_2 . Here we took $U_n = 0.002\ atm-cm$ [26]. c_1, c_2, c_3, h_1 and h_2 are parameters depending on the total column amount precipitate water U_W with $U_W = m_w.w$ [25]. λ_{e_1} and λ_{e_2} are the effective aerosol wavelength in each band[24]. Concerning the turbidity data, we considered $\alpha_1 = \alpha_2 = 1.3$ and $\beta_1 = \beta_2 = \beta$.

2.2. The data used

The satellite-derived data of hourly direct normal radiation considered in this work were Generated-using CAMS-rad service from 2004 up to December 2018. This data has been constructed for the actual weather conditions as well as for clear-sky conditions from images acquired by the Meteosat series of satellites. The coverage area is Europe, Africa, the Atlantic Ocean and the Middle East. The resolution distance is 3 km at Nadir and is 4 to 5 km in latitude 45°. The data are freely available from the web site Soda service. The turbidity data, namely the Angstrom's coefficient and Linke turbidity, for reference days in this work were considered approximatively to the mean monthly values shown in Table.2 and also available at the SoDa Service [27]. The hourly ambient temperature and relative humidity were extracted for each reference days and sites from the Soda service. A polynomial fit was used to obtain correlations describing their variations for the sunny period of the day versus true solar time (TST). The overall of the correlations is tabulated in Appendix I.

Table 2. Monthly mean values of Angstrom's coefficient β and factor turbidity of Linke T_L [27]

Locations	Months	β	T_L
Errachidia	June	0.12	4.6
	December	0.06	3.4
	March	0.03	2.8
	September	0.15	5.2
Ouarzazate	June	0.12	4.6
	December	0.07	3.5
	March	0.07	3.5
	September	0.13	4.8
Guelmime	June	0.08	3.8
	December	0.05	3.2
	Mars	0.06	3.4
	September	0.08	3.9
Tendrara	June	0.08	4.0
	December	0.03	4.3
	Mars	0.01	2.5
	September	0.10	4.3

2.3. Statistical comparison method

The Model's performances are analyzed using the most common error metrics used in the literature, mainly the Relative Mean Bias Error (rMBE), the Relative Root Mean Square Error (rMSE) and the determination coefficient R^2. They are defined as follows[28]-[29]-[30]:

$$rMBE = \left(\frac{1}{n\,\overline{m}} \sum_{i=1}^{n} \left(c_i - m_i \right) \right) \tag{55}$$

$$rRMSE = \left(\frac{1}{\overline{m}} \sqrt{\frac{1}{n} \sum_{i=1}^{n} (c_i - m_i)^2} \right) \tag{56}$$

$$R^2 = \frac{\left[\sum_{i=1}^{n} \left(m_i - \overline{m} \right)\left(c_i - \overline{c} \right) \right]^2}{\sum_{i=1}^{n} \left(m_i - \overline{m} \right)^2 \left(c_i - \overline{c} \right)^2} \tag{57}$$

Where c_i is a calculated value by a given model, m_i is the measured value at time i, n is the total number of observations, $\overline{m}$ and $\overline{c}$ are the means of the total measured and the calculated data points, respectively.

A model designed to compute hourly normal solar irradiance provides a good performance if the *rMBE*, *rRMSE* have as low values as possible and R^2 near at 1.

In addition to the error metrics, the paired *t-test* is also used to make a decision for a given level of significance α, whether the means of the two dependents groups of results are different. The observed value t_{ob} of the t-test is calculated using the following formula[31]:

$$t_{ob} = \overline{d} / (S_d / \sqrt{n}) \tag{58}$$

Where $\overline{d} = \overline{m} - \overline{c}$ and $\overline{c}$ is the mean over all calculated data points for a given model and S_d the standard deviation estimated from a sample of the differences: $d_i = m_i - c_i$. It is expressed as:

$$S_d = \frac{1}{n-1} \sum_{i=1}^{n} \left(d_i - \overline{d} \right)^2 \tag{60}$$

The two-sided hypothesis tested are H_0 (the two samples of data are conform: $\overline{d} = 0$) against the opposite hypothesis H_1 (the two samples of data are different: $\overline{d} \neq 0$). The p-value is the lowest level of significance required to reject a null hypothesis using the data provided. [31]. We computed the p-value using statistical software. The decision about the null hypothesis is made by comparison of the p-value and α .if the p-value is more than α , we accept the hypothesis null, and we judged that the difference between calculated values and measured ones is statistically insignificant for a level of significance α . Here, we used the usual values of level of significance 0.1%; 1%; and 5%. The p-value is computed using the free statistical software "R". Table.3 shows categories of models used in the work. this classification method was used by Badescu et al [32] and then adopted by Engerer and Mills[33].

Finally, to facilitate the distinction between the different models, we assigned a weighting factor to each category, +3 for "excellent", +2 for "good", +1 for "average", and 0 for "poor", Then we calculated a score for each model. Thus, an excellent model will have a score of 36, a good model will have a score of 24, and average will have a score of 12. Intermediate scores are obviously possible.

Table 3. The three performances categories for the statistical parameters used

Model	|rMBE|	rRMSE	R²
Poor	≥ 10%	≥ 15%	≤ 0.80
Average	≥ 5%	≥ 10%	≤ 0.90
Good	≥ 2%	≥ 5%	≤ 0.97
Excellent	< 2%	< 5%	> 0.97

3. Results and discussion

By simply looking at the curves in Fig.1 and Fig.2 and Fig.3 and Fig.4, it appears that some models show fewer discrepancies from the mean measured values than others. This statement depends on the reference day and the studied site For Ouarzazate site, as shown in Fig.1, the Molineaux and the REST2 models, for March 20, give closer estimates. In contrast to September 23 and June 21, the Bird and the Linke-Kasten models are the closest ones. For December 21, the Hoyt model and the Paltridge model give results that are more convincing.

In the case of Errachidia site, as seen in Fig.2 the Bird model and the Molineaux are more accurate for June 21. In contrast, for December 21, the Atwater & Ball and the Hoyt models are more accurate. For March 20, the REST2 and the Molineaux models coincide very well with the measured values. For September 23, the Ineichen & Perez Model, the bird Model, and the Linke-Kasten Models are more performant.

Figure.3 shows that the REST2 and Molineaux models give very good estimates for Guelmime site and for June 21. The same models give relatively acceptable results for September 23. On the contrary, for December 21, Bird Model, Ineichen & Perez model, and Linke-Kasten give values in very good agreements with measured ones. For March 20, no parametric model gives calculation results showing acceptable discrepancies with CAMS-rad values.

For the site of Tendrara and for June 21, we note as shown in Fig.4 that the Molineaux and REST2 models give results that perfectly match the measured values. For September 23, the Bird and Ineichen & Perez models are producing very convincing results. On the other hand, for 20 March all models give results of calculations more distinguished from the measured values.

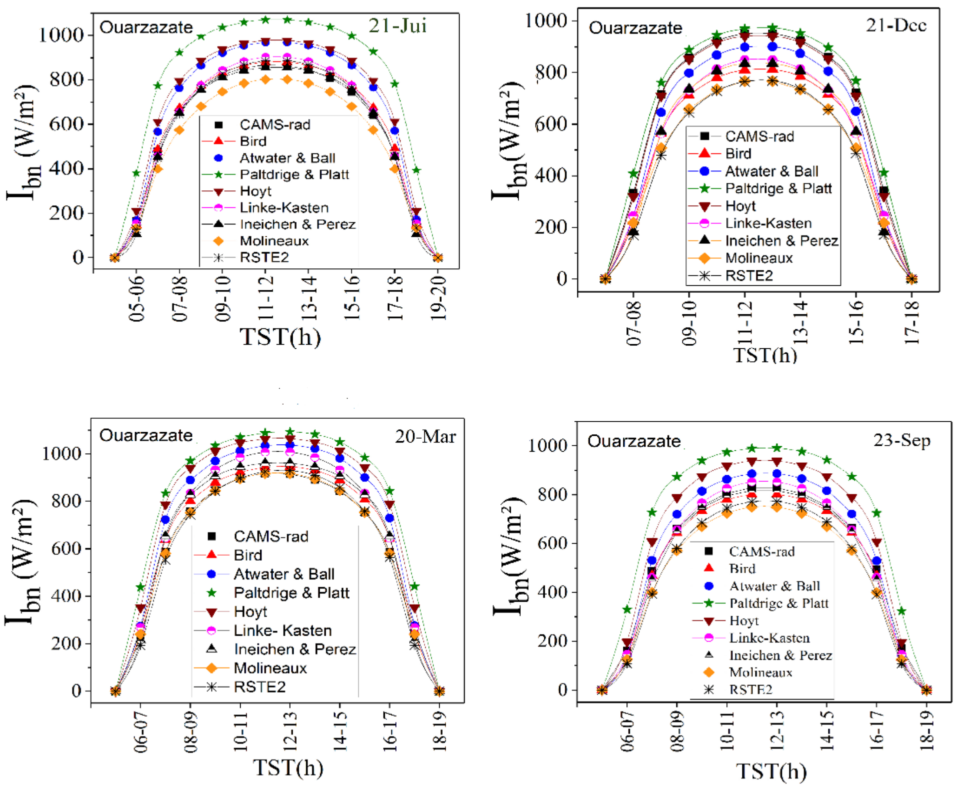

Fig. 1. Direct normal irradiance estimated for the two equinoxes and the two solstices using eight parametric models and derived – Satellite data for Ouarzazate.

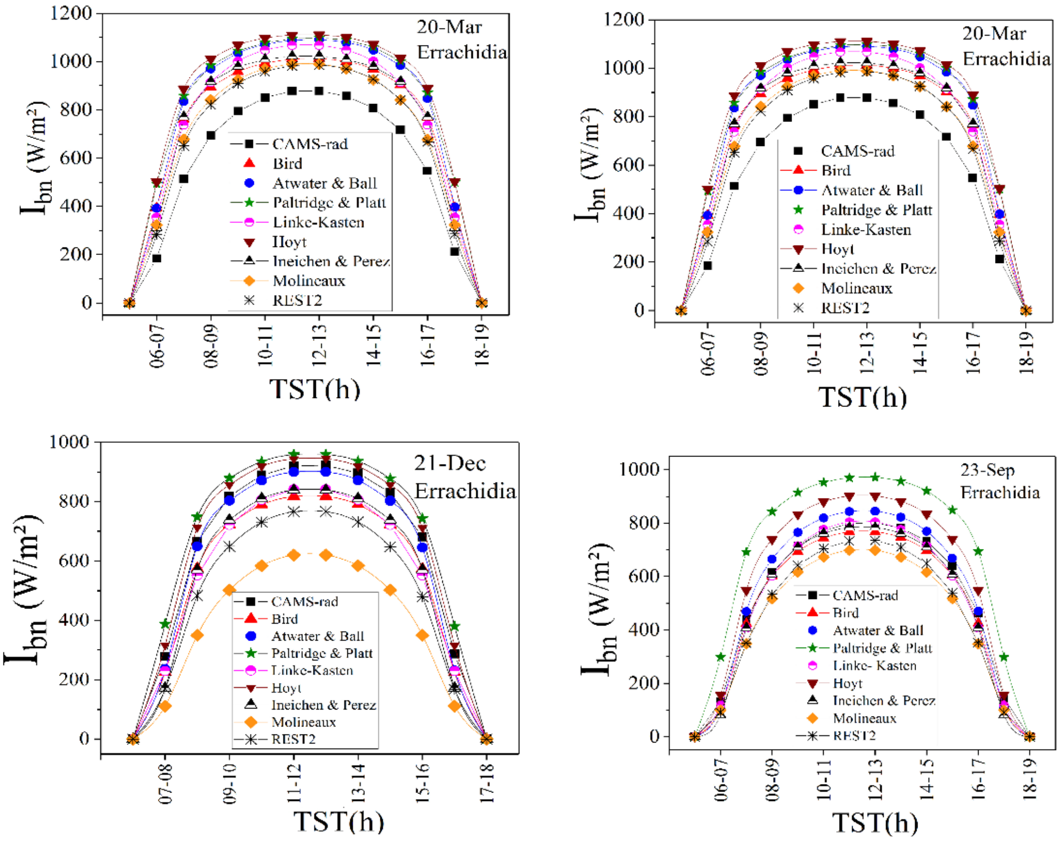

Fig. 2. Direct normal irradiance estimated for the two equinoxes and the two solstices using eight parametric models and derived – Satellite data for Errachidia.

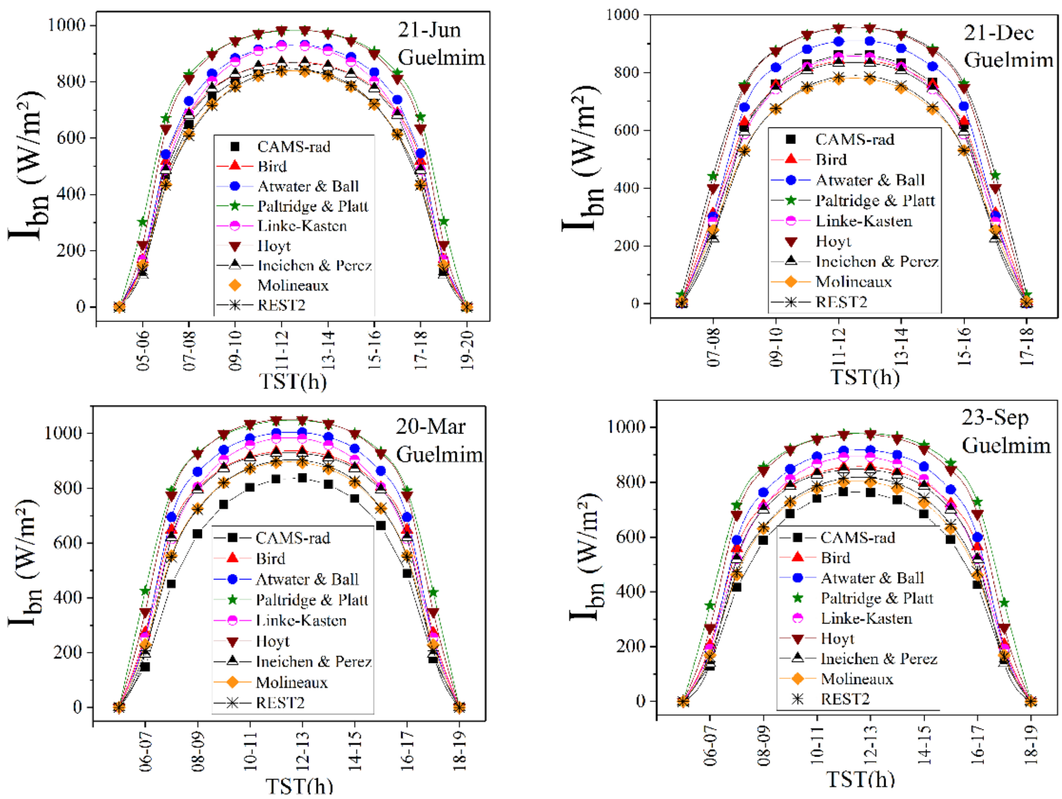

Fig. 3. Direct normal irradiance estimated for the two equinoxes and the two solstices using eight parametric models and derived – Satellite data for Guelmim.

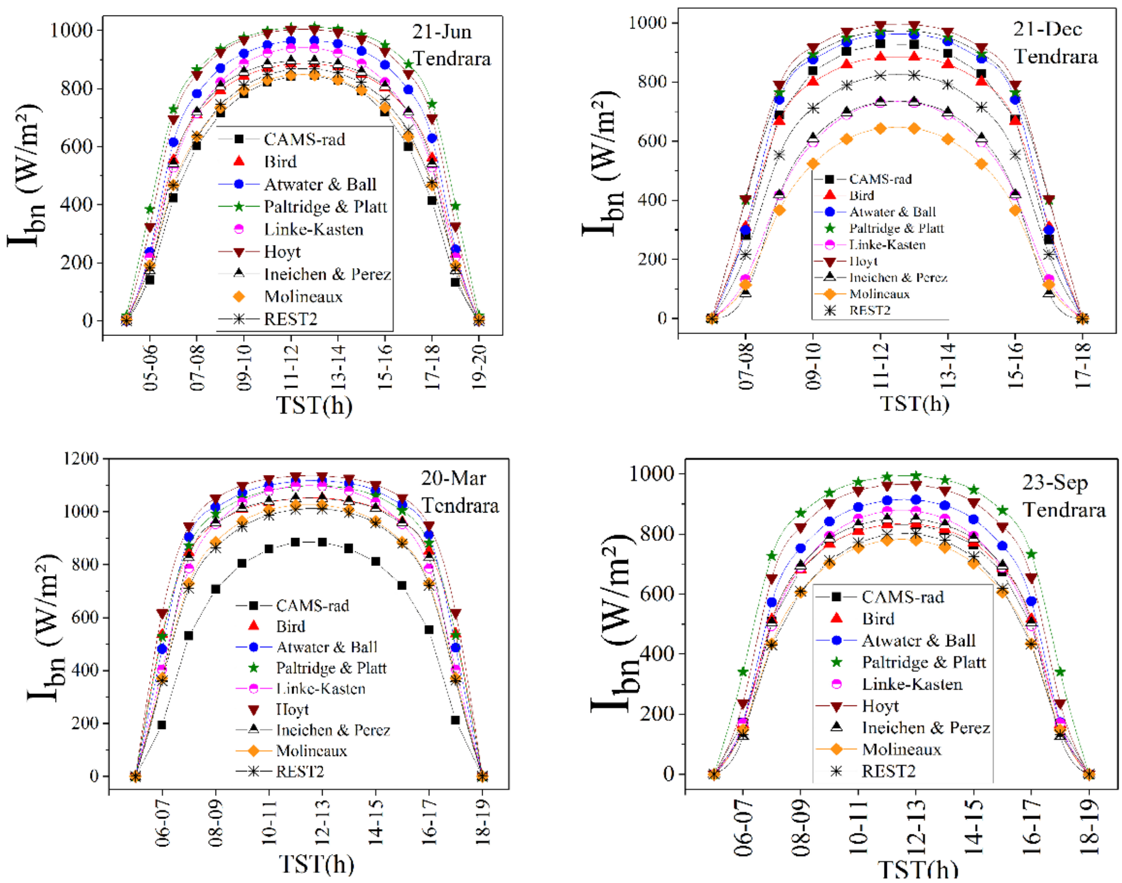

Fig. 4. Direct normal irradiance estimated for the two equinoxes and the two solstices using eight parametric models and derived – Satellite data for Tendrara.

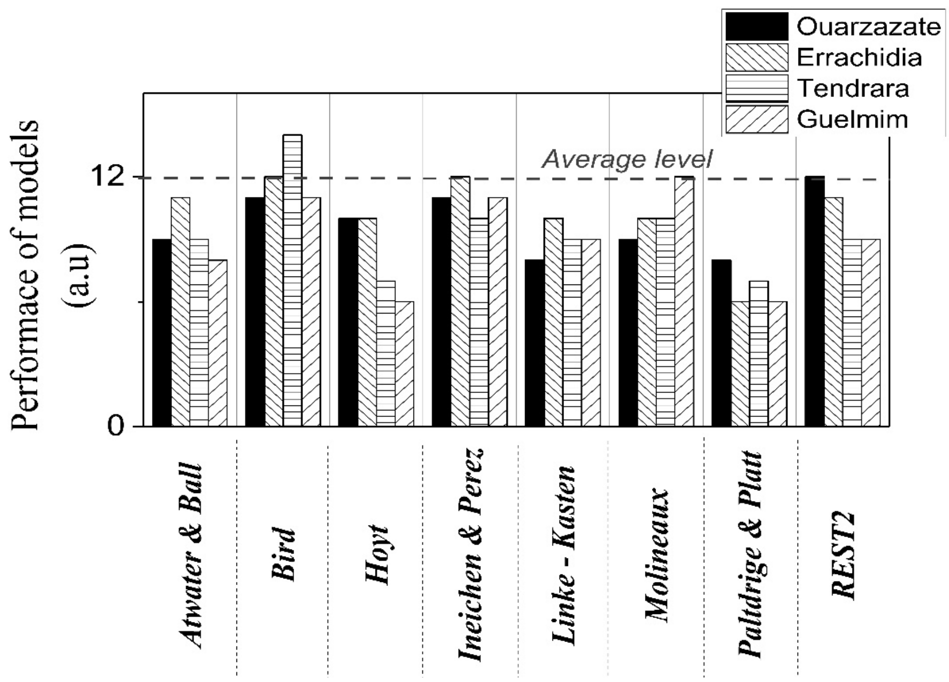

Fig. 5. Evaluation of performance score of different models by locations

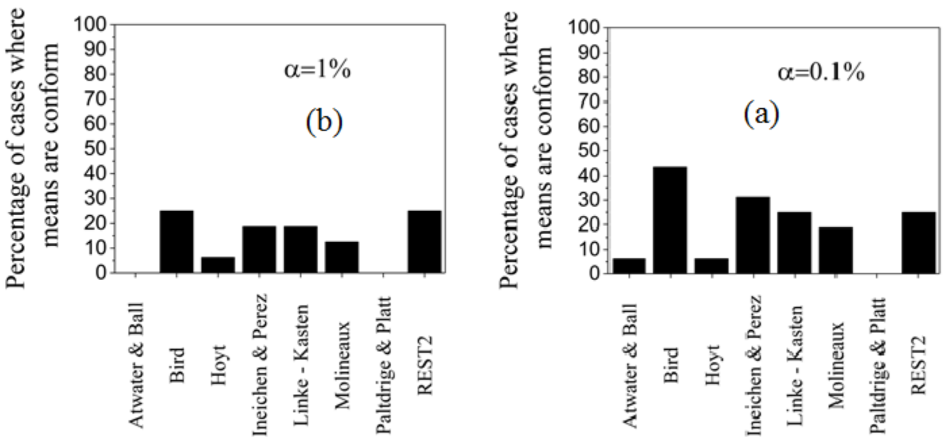

Fig. 6. Percentage of statistically significant cases with $\alpha = 0.1\%$ (a) and $\alpha = 1\%$ (b) for different models

4. Conclusion

The performance of each model at each site and for each reference day was first calculated by determining the overall relative mean bias error, the relative root mean square error and the determination coefficient. The models were classified according to their performance into four categories: "excellent", "good", "average" and "poor". Finally, with the intention of generalizing to the entire Moroccan arid zone, we have determined the most robust model or models giving better estimates in the four selected sites.

Relatively satisfactory results have been obtained for the Bird model followed by Ineichen & Perez, Molineaux, and REST2 Models. The calculated statistical parameters state that the Bird model gives good estimates results against other models. 62.5% of satisfactory values of *rMBE* ranging between 0 and 6%; 25% of average values of *rRMSE* ranging between 11% and 14%, and 62.5% of good values of R^2 ranging between 0.90 and 0.96 are obtained for this model. Our comparison of conformity of means, calculated and measured, using the paired t-test, achieves that the Bird model displays for a level of significance $\alpha = 0.1\%$ the highest Percentage of cases with conforming means, almost the half of tested cases. This percentage decreases to the quarter cases when $\alpha = 1\%$. One note that for a level of significance most serious, $\alpha = 5\%$ for example, value usually used for this type of comparison, no Model produce conforming means to the measured one. Finally, we note that the percentages achieved remains below the attempted results. The elaboration of a new simpler broadband model for arid Moroccan zone seems to be of great importance.

APPENDIX I:

Ambient temperature and relative humidity correlations versus Time solar true *t* in (h) determined for of the corresponding sites and for the sunny period of the day on the basis of the data from 01/10/2004 To 01/10/2018[34] . R^2 is the coefficient of determination of the polynomial fit realized.

Locations	Days	T(K)	*RH* (%)
Ouarzazate	21-Jun	$T = 0.0021t^4 - 0.1175t^3 + 2.1294t^2 - 13.503t + 291.58; \quad R^2 = 0.9945$	$RH = -0.0351t^3 + 1.8219t^2 - 29.72t + 166.32;\ R^2 = 0.9892$
	21-Dec	$T = 0.0046t^4 - 0.2513t^3 + 4.6553t^2 - 33.506t + 357.2;\ R^2 = 0.9923$	$RH = -0.0182t^4 + 0.9711t^3 - 17.781t^2 + 127.68t - 240.9;\ R^2 = 0.9905$
	20-Mar	$T = 0.003t^4 - 0.1618t^3 + 2.8799t^2 - 18.545t + 316.46;\ R^2 = 0.9905$	$RH = -0.0079t^4 + 0.4207t^3 - 7.1078t^2 + 39.232t + 8.8964;\ R^2 = 0.9741$
	23-Sept	$T = 0.0023t^4 - 0.1206t^3 + 2.0678t^2 - 12.003t + 309.16;\ R^2 = 0.9826$	$RH = 0.0228t^3 - 0.319t^2 - 4.5405t + 82.727;$
	21-Jun	$T = -0.237t^2 + 6.7807t + 258.7;\ R^2 = 0.9913$	$RH = -0.0098t^3 + 0.9116t^2 - 20.199t + 142.67;\ R^2 = 0.9868$
	21-Dec	$T = 0.0049t4 - 0.2586t3 + 4.681t2 - 32.792t + 351.71; \quad R^2 = 0.9906$	$RH = -0.0158t^4 + 0.8201t^3 - 14.447t^2 + 97.074t - 136.58;\ R^2 = 0.9842$

Errachidia	20-Mar	$T = -0.2585t^2 + 7.2733t + 241.48;\ R^2 = 0.991$	$RH = 0.9754t^2 - 27.374t + 211.36;\ R^2 = 0.9842$
	23-Sept	$y = -0.2552t^2 + 7.1755t + 252.11;\ R^2 = 0.9929$	$RH = 0.6624t^2 - 18.367t + 149.82\ R^2 = 0.9852$
Guelmime	21-Jun	$T = -0.0046t^3 - 0.0301t^2 + 3.4825t + 272.77\ ;\ R^2 = 0.9829$	$RH = 0.7955t^2 - 21.651t + 180.59;\ R^2 = 0.9908$
	21-Dec	$T = 0.0042t^4 - 0.2309t^3 + 4.3228t^2 - 31.866t + 363.19$	$RH = -0.0106t^4 + 0.5814t^3 - 10.675t^2 + 74.439t - 103.73;\ R^2 = 0.9877$
	20-Mar	$T = -0.0089t^3 + 0.1243t^2 + 1.8042t + 270.9;\ R^2 = 0.9843$	$RH= -0.0075t^4 + 0.4254t^3 - 7.7911t^2 + 51.277t - 35.745;\ R^2 = 0.9905$
	23-Sept	$T = 0.0026t^4 - 0.1445t^3 + 2.6354t^2 - 18.014t + 333.49$	$RH= -0.0088t^4 + 0.4861t^3 - 8.7674t^2 + 57.062t - 41.678;\ R^2 = 0.9915$
Tendrara	21-Juin	$T = -0.3013t^2 + 8.4437t + 246.78;\ R^2 = 0.9903$	$RH=0.0128t^4 - 0.6841t^3 + 14.016t^2 - 131.43t + 494.87;\ R^2 = 0.9952$
	21-Dec	$T = 0.0086t^4 - 0.4548t^3 + 8.4762t^2 - 64.849t + 449.26;\ R^2 = 0.984$	$RH = -0.0321t^4 + 1.676t^3 - 30.827t^2 + 231.84t - 527.99;\ R^2 = 0.986$
	20-Mar	$T = -0.2776t^2 + 7.526t + 238.73\ R^2 = 0.9804$	$RH = 1.0739t^2 - 29.826t + 236.66\ R^2 = 0.9893$
	23-Sept	$T = -0.3076t^2 + 8.4377t + 243.28\ R^2 = 0.9825$	$RH = 0.9463t^2 - 25.913t + 200.23\ R^2 = 0.9885$

APPENDIX II : Evaluation of the clear sky direct normal irradiance models for Ouarzazate, Errachidia, Guelmime and Tendrara, respectively, with *rMBE*, *rRMSE*, R^2 and *paired t-test* calculated in each instance.

Ouarzazate	*Date*	$\lvert rMBE \rvert$ %	*rRMSE* %	R^2	t_{ob}	*p-value*
Bird Model	20-Mar	5	21	0.852	3.37	0.001
	23-Sep	4	22	0.868	-2.43	0.016
	21-Jun	2	16	0.916	2.10	0.037
	21-Dec	18	21	0.948	-21.51	0.000
Atwater and Ball Model	20-Mar	16	27	0.850	10.42	0.000
	23-Sep	7	23	0.867	3.99	0.000
	21-Jun	14	22	0.915	12.39	0.000
	21-Dec	9	13	0.949	-9.98	0.000
Paltridge & Platt model	20-Mar	29	36	0.848	18.77	0.000
	23-Sep	30	37	0.861	17.92	0.000
	21-Jun	37	41	0.907	32.05	0.000
	21-Dec	5	11	0.949	6.12	0.000
Linke-Kasten	20-Mar	10	23	0,853	6,76	0,000
	23-Sep	17	28	0.866	9.78	0.000
	21-Jun	3	16	0.916	2.36	0.019
	21-Dec	15	19	0.945	-17.70	0.000
Hoyt	20-Mar	23	31	0.849	14.83	0.000
	23-Sep	17	28	0.866	9.78	0.000
	21-Jun	18	25	0.913	15.91	0.000
	21-Dec	1	10	0.949	-1.52	0.131
Ineichen & Perez	20-Mar	6	22	0.850	4.13	0.000
	23-Sep	4	22	0.868	-2.22	0.028
	21-Jun	2	16	0.916	-1.69	0.093
	21-Dec	17	20	0.949	-20.22	0.000
Molineaux	20-Mar	0	20	0.853	-0.02	0.980
	23-Sep	13	25	0.867	-7.58	0.000
	21-Jun	10	19	0.916	-8.66	0.000
	21-Dec	24	26	0.944	-26.22	0.000
REST2	20-Mar	1	21	0.853	-0.73	0.466
	23-Sep	11	24	0.866	-6.82	0.000
	21-Jun	0	16	0.917	0.36	0.719
	21-Dec	26	28	0.944	-29.71	0.000

Errachidia	Date	$\lvert rMBE \rvert$ %	*rRMSE* %	R^2	t_{ob}	*p-value*
Bird Model	March20th	4	39	0.851	16.05	0.000
	September23th	5	19	0.904	3.38	0.001
	June 21th	5	14	0.953	6.08	0.000
	December21th	13	17	0.943	12.89	0.000
Atwater & Ball model	March20th	47	49	0.846	21.86	0.000
	September23th	5	20	0.904	3.11	0.002
	June 21th	16	21	0.951	17.58	0.000
	December21th	4	12	0.943	3.86	0.000
Paltridge & Platt model	March20th	53	53	0.849	24.35	0.000
	September23th	33	38	0.897	22.07	0.000
	June 21th	37	40	0.943	38.48	0.000
	December21th	9	15	0.943	8.47	0.000
Linke-Kasten model	March20th	37	41	0.855	17.87	0.000
	September23th	3	19	0.902	1.82	0.070
	June 21th	9	16	0.955	10.95	0.000
	December21th	12	17	0.939	12.18	0.000
Hoyt	March20th	56	55	0.846	25.63	0.000
	September23th	15	25	0.902	10.25	0.000
	June 21th	25	28	0.948	27.23	0.000
	December21th	4	12	0.943	4.37	0.000
Ineichen & Perez	March20th	4	39	0.844	15.60	0.000
	September23th	5	20	0.904	3.21	0.002
	June 21th	6	14	0.952	6.91	0.000
	December21th	13	17	0.943	13.08	0.000
Molineaux	March20th	25	33	0.855	11.79	0.000
	September23th	16	25	0.902	10.82	0.000
	June 21th	4	13	0.954	4.28	0.000
	December21th	40	42	0.932	33.31	0.000
REST2	March20th	22	31	0.856	10.48	0.000
	September23th	13	23	0.902	8.77	0.000
	June 21th	1	12	0.954	1.22	0.225
	December21th	22	25	0.939	21.63	0.000
Guelmime	**Date**	$\lvert rMBE \rvert$ %	*rRMSE* %	R^2	t_{ob}	*p-value*
Bird Model	March20th	21	31	0.858	12.39	0.000
	September23th	19	34	0.819	9.37	0.000
	June 21th	6	18	0.9212	5.32	0.000
	December21th	0	12	0.945	0.45	0.652
Atwater and Ball Model	March20th	29	37	0.856	16.53	0.000
	September23th	27	39	0.818	12.51	0.000
	June 21th	13	22	0.912	10.60	0.000
	December21th	7	13	0.944	7.72	0.000
Paltridge & Platt model	March20th	42	48	0.855	24.32	0.000
	September23th	44	52	0.814	21.26	0.000
	June 21th	27	32	0.908	22.14	0.000
	December21th	19	22	0.945	18.44	0.000
Linke-Kasten	March20th	23	32	0.863	13.53	0.000
	September23th	20	34	0.823	9.54	0.000
	June 21th	10	20	0.914	8.18	0.000
	December21th	2	11	0.944	1.98	0.049
Hoyt	March20th	40	46	0.853	22.82	0.000
	September23th	39	49	0.815	18.65	0.000
	June 21th	24	29	0.909	19.42	0.000
	December21th	17	20	0.944	17.46	0.000
Ineichen & Perez	March20th	18	29	0.856	10.09	0.000
	September23th	14	32	0.819	6.91	0.000
	June 21th	4	18	0.912	3.44	0.001
	December21th	4	12	0.945	4.62	0.000
	March20th	11	25	0.864	6.78	0.000
	September23th	7	28	0.823	3.42	0.001

Molineaux	June 21th	2	17	0.914	1.31	0.191
	December21th	4	12	0.945	4.62	0.000
REST2	March20th	11	25	0.864	6.58	0.000
	September23th	9	29	0.823	4.26	0.000
	June 21th	2	17	0.914	1.60	0.111
	December21th	11	16	0.944	11.30	0.000
Tendrara	**Date**	$\lvert rMBE \rvert$ %	*rRMSE %*	R^2	t_{ob}	***p-value***
Bird Model	March20th	36	41	0.878	22.76	0.000
	September23th	0	14	0.933	0.44	0.661
	June 21th	13	20	0.936	12.81	0.000
	December21th	3	11	0.956	2.85	0.005
Atwater and Ball Model	March20th	42	47	0.870	28.43	0.000
	September23th	11	18	0.932	9.39	0.000
	June 21th	24	28	0.932	23.33	0.000
	December21th	5	12	0.955	6.28	0.000
Paltridge & Platt model	March20th	41	45	0.878	27.07	0.000
	September23th	29	33	0.928	26.37	0.000
	June 21th	37	41	0.927	33.16	0.000
	December21th	10	15	0.956	10.88	0.000
Linke-Kasten	March20th	33	38	0.882	23.68	0.000
	September23th	3	15	0.932	2.80	0.006
	June 21th	16	21	0.941	16.78	0.000
	December21th	29	31	0.945	29.45	0.000
Hoyt	March20th	49	53	0.875	31.11	0.000
	September23th	21	25	0.930	18.38	0.000
	June 21th	33	36	0.929	31.20	0.000
	December21th	13	17	0.956	14.23	0.000
Ineichen & Perez	March20th	31	37	0.869	20.86	0.000
	September23th	1	15	0.933	0.67	0.507
	June 21th	13	19	0.934	12.36	0.000
	December21th	30	32	0.951	13.62	0.000
Molineaux	March20th	24	31	0.883	17.09	0.000
	September23th	9	17	0.932	8.17	0.000
	June 21th	4	15	0.941	3.98	0.000
	December21th	38	40	0.945	34.45	0.000
REST2	March20th	22	29	0.883	15.66	0.000
	September23th	8	16	0.931	7.01	0.000
	June 21th	6	15	0.941	6.30	0.000
	December21th	14	18	0.954	15.86	0.000

References

[1] J. Bahraoui-Buret, M. N. Bargach, and M. L. Ben Kaddour, Le gisement Solaire Marocain. Société marocaine des éditeurs réunis, 1983.

[2] “MOROCCAN SOLAR ENERGY PROGRAM,” Ministry of Energy, Mines, and Sustainable Development, 08-Jan-2019. [Online]. Available: http://www.mem.gov.ma/SitePages/GrandChantiersEn/DEREESolarEnergy.aspx#.

[3] S. AlYahya and M. A. Irfan, “New solar radiation Atlas for Saudi Arabia,” in 2014 International Conference on Renewable Energy Research and Application, pp. 245–249, 19-22 October. 2014.

[4] L. Cirocco, M. Belusko, F. Bruno, J. Boland, and P. Pudney, “Optimisation of storage for concentrated solar power plants,” Challenges, vol. 5, no. 2, pp. 473–503, December 2014.

[5] Moroccan Agency For Sustainable Energy, “Atlas de la resource solaire du maroc,” 10-Sep-2018. [Online]. Available: https://solaratlas.masen.ma/. [Accessed: 19-Oct-2018].

[6] M. Demirtas, M. Yesilbudak, S. Sagiroglu, and I. Colak, “Prediction of solar radiation using meteorological data,” in 2012 International Conference on Renewable Energy Research and Applications, Nagasaki, Japan, pp. 1–4, 11-14 November. 2012

[7] M. Marchand, A. Ghennioui, E. Wey, and L. Wald, “Comparison of several satellite-derived databases of surface solar radiation against ground measurement in Morocco,” Advances in Science and Research, vol. 15, pp. 21–29, April 2018.

[8] L. T. Wong and W. K. Chow, “Solar radiation model,” Applied Energy, vol. 69, no. 3, pp. 191–224, July 2001.

[9] R. E. Bird, "A simple, solar spectral model for direct-normal and diffuse horizontal irradiance," Solar Energy, vol. 32, no. 4, pp. 461–471, 1984.

[10] M. Iqbal, An Introduction To Solar Radiation. Elsevier Science, 2012.

[11] R. E. Bird and R. L. Hulstrom, "A simplified clear sky model for direct and. diffuse insolation on horizontal surfaces," Solan Energy Research Institute - A Division of Midwest Research Institute, February 1981.

[12] F. Kasten, "A new table and approximation formula for the relative optical air mass," Archiv für Meteorologie, Geophysik und Bioklimatologie Serie B, vol. 14, no. 2, pp. 206–223, September 1965.

[13] Y. Mizuno et al., "Improvement of solar radiation model based on physical parametrization," in 2015 International Conference on Renewable Energy Research and Applications, Palermo, Italy, pp. 789–792, 22-25 November. 2015

[14] T. K. Van Heuklon, "Estimating atmospheric ozone for solar radiation models," Solar Energy, vol. 22, no. 1, pp. 63–68, 1979.

[15] A. Chiron de la Casinière, Le rayonnement solaire Dans l'environnement terrestre. Paris, 2003.

[16] M. A. Atwater and J. T. Ball, "A numerical solar radiation model based on standard meteorological observations," Solar Energy, vol. 21, no. 3, pp. 163–170, 1978.

[17] G. W. Paltridge and C. M. R. Platt, Radiative Processes in Meteorology and Climatology. Amsterdam: Elsevier Scientific Pub. Co., 1976.

[18] R. Bird and R. Hulstrom, "Direct insolation models," SERI/TR-335-344, 5626683, January. 1980.

[19] P. Ineichen and R. Perez, "A new airmass independent formulation for the Linke turbidity coefficient," Solar Energy, vol. 73, no. 3, pp. 151–157, September 2002.

[20] A. El-Abidi, S. Yadir, F. Chanaa, M. Benhmida, H. Bousseta, and H. Ezzaki, "Modeling and Simulation of a Modified Solar Air Heater Destined to Drying the Gelidium Sesquipedale," International Journal Of Renewable Energy Research, vol. 8, no. 4, pp. 2003–2013, December. 2018.

[21] F. Kasten, "The Linke turbidity factor based on improved values of the integral Rayleigh optical thickness," Solar Energy, vol. 56, no. 3, pp. 239–249, March 1996.

[22] D. V. Hoyt, "A model for the calculation of solar global insolation," Solar Energy, vol. 21, no. 1, pp. 27–35, 1978.

[23] B. Molineaux, P. Ineichen, and J. J. Delaunay, "Direct luminous efficacy and atmospheric turbidity-improving model performance," Solar Energy,Vol. 55, no. 2, pp. 125-137 August 1995.

[24] C. A. Gueymard, "REST2: High-performance solar radiation model for cloudless-sky irradiance, illuminance, and photosynthetically active radiation – Validation with a benchmark dataset," Solar Energy, vol. 82, no. 3, pp. 272–285, March. 2008.

[25] C. Gueymard, "A two-band model for the calculation of clear sky solar irradiance, illuminance, and photosynthetically active radiation at the earth's surface," Solar Energy, vol. 43, no. 5, pp. 253–265, 1989.

[26] C. A. Gueymard, "Parameterized transmittance model for direct beam and circumsolar spectral irradiance," Solar Energy, vol. 71, no. 5, pp. 325–346, November 2001.

[27] "Solar Energy Services for professionals." [Online]. Available: http://www.soda-pro.com. [Accessed: 19-Oct-2018].

[28] H. Loutfi, A. Bernatchou, and R. Tadili, "Generation of horizontal hourly global solar radiation from exogenous variables using an artificial neural network in Fes (Morocco)," International Journal of Renewable Energy Research, vol. 7, no. 3, pp. 11, 2017.

[29] K. Gairaa, F. Chellali, S. Benkaciali, Y. Messlem, and K. Abdallah, "Daily global solar radiation forecasting over a desert area using NAR neural networks comparison with conventional methods," in 2015 International Conference on Renewable Energy Research and Applications, Palermo, pp. 567–571, 22-25 November. 2015

[30] A. Alzahrani, P. Shamsi, M. Ferdowsi, and C. Dagli, "Solar irradiance forecasting using deep recurrent neural networks," in 2017 IEEE 6th International Conference on Renewable Energy Research and Applications, San Diego, CA, USA , pp. 988–994, 5-8 November 2017

[31] Douglas C. Montgomery and G. C. Runger, Applied Statistics and Probability for Engineers, Fifth Edition. USA: John Wiley & Sons, 2011.

[32] V. Badescu et al., "Accuracy analysis for fifty-four clear-sky solar radiation models using routine hourly global irradiance measurements in Romania," Renewable Energy, vol. 55, pp. 85–103, July 2013.

[33] N. A. Engerer and F. P. Mills, "Validating nine clear sky radiation models in Australia," Solar Energy, vol. 120, pp. 9–24, October 2015.

[34] Global Modeling and Assimilation Office (GMAO) (2015), MERRA-2 tavg1_2d_slv_Nx: 2d,1-Hourly,Time-Averaged,Single-Level,Assimilation,Single-Level Diagnostics V5.12.4, Greenbelt, MD, USA, Goddard Earth Sciences Data and Information Services Center (GES DISC), Accessed[21-oct-2018] DOI:10.5067/VJAFPLI1CSIV.